# Differential elastic-scattering measurements of $Xe^+$ on Xe and $Ar^+$ on Ar in the 20–340-eV range*

P. R. Jones,† G. M. Conklin, D. C. Lorents, and R. E. Olson
*Stanford Research Institute, Menlo Park, California 94025*

(Received 13 February 1974)

Relative measurements of the differential cross section for elastic scattering of $Xe^+$ on Xe and $Ar^+$ on Ar are reported in the energy range 20–340 eV and the angular range 1–15 deg (lab). The data are presented in terms of the reduced cross section $\rho(\theta) \equiv \theta \sin\theta\, \sigma(\theta)$ and the reduced angle $\tau \equiv E\theta$. The $\rho$-vs-$\tau$ plots for $Xe^+$ on Xe show complex oscillations which we attribute primarily to phase interference in scattering from three coherent pairs of *gerade-ungerade* potential curves. The six states involved are the electronic fine-structure states of $Xe_2^+$, four of which dissociate to $Xe + Xe^+(^2P_{3/2})$, and the other two to $Xe + Xe^+(^2P_{1/2})$. At larger values of $\tau$ the elastic scattering pattern is further complicated by potential-curve crossings and excitation to higher states, while at smaller $\tau$ potential wells give rise to two rainbow peaks. We have resolved two oscillatory patterns in the data, from which we have determined two difference potentials for $Xe_2^+$, $\Delta V_{JM}(R) \equiv |V_{JMg}(R) - V_{JMu}(R)|$: $\Delta V_{3/2,3/2} = 23e^{-1.23R}$, $3.5 \lesssim R \lesssim 5.5$; and $\Delta V_{1/2,1/2} = 2.0e^{-0.788R}$, $5 \lesssim R \lesssim 6.5$, in a.u. The $Ar^+$ on Ar data are in excellent agreement with scattering calculations based upon *ab initio* computations of the $\Pi_u$ and $\Pi_g$ potentials of $Ar_2^+$.

## I. INTRODUCTION

During the past decade collision-spectroscopy studies of $Ne^+$ on Ne and $Ar^+$ on Ar have demonstrated the dominant role of coherent $\Pi_g$ and $\Pi_u$ molecular electronic states in producing the prominent interference pattern seen in differential measurements of both the direct elastic and charge-exchange scattering.[1–3] The $\Sigma_g$ and $\Sigma_u$ states have been identified as being responsible for a secondary oscillation in the $Ne^+$-on-Ne differential cross sections[4] and may produce similar oscillations, too rapid to detect with ordinary angular resolution, in $Ar^+$-on-Ar scattering.

The six molecular fine-structure states, which arise from the spin-orbit interaction, have not been identified as playing a part in producing the observable features of the scattering patterns for these systems. The spin-orbit interaction energy, as indicated by the splitting between the $^2P_{3/2}$ and $^2P_{1/2}$ states, is about 0.1 and 0.2 eV for $Ne^+$ and $Ar^+$, respectively. At collision energies above 100 eV, the long-range coupling during the encounter is large enough to completely couple the fine-structure states; therefore the spin-orbit interaction can be neglected, giving rise to a pair of doubly degenerate $\Pi$ states and a pair of $\Sigma$ states as the effective interaction potentials for the collision.

The heavier noble gases have stronger spin-orbit interactions, however; the $^2P_{1/2}$-$^2P_{3/2}$ splitting is 0.67 and 1.31 eV for $Kr^+$ and $Xe^+$, respectively. The stronger spin-orbit interactions in these systems also pervade the molecular states that govern the scattering. Consequently, the molecular fine-structure states of these systems may remain adiabatic for elastic scattering at energies up to about 100 eV. The interference pattern should contain three oscillations instead of the two which result when the spin-orbit interaction is negligible, provided there are both $^2P_{3/2}$ and $^2P_{1/2}$ ions present in the ion beam.

The six fine-structure potential-energy curves of $Xe_2^+$ are shown in Fig. 1, taken from the work of Johnson.[5] (The common repulsive term in the interaction potential has been omitted, as have some small common attractive terms.) For large internuclear separation $R$, $(J_a, J_b)$ coupling dominates with $J_a(\text{atom}) = 0$ and $J_b(\text{ion}) = \frac{3}{2}$ or $\frac{1}{2}$, so that $\vec{J} = \vec{J}_a + \vec{J}_b$ reduces to $J = J_b$. The projection of angular momentum on the internuclear axis $M$ is a good quantum number at all separations, as is the parity $P$—*gerade* or *ungerade*—so that the states may be designated $(J, M, P)$. In this scheme the coherent pairs of states in ion-atom scattering are $(\frac{1}{2}, \frac{1}{2}, g)$ and $(\frac{1}{2}, \frac{1}{2}, u)$—the upper pair: $(\frac{3}{2}, \frac{3}{2}, u)$ and $(\frac{3}{2}, \frac{3}{2}, g)$; $(\frac{3}{2}, \frac{1}{2}, g)$ and $(\frac{3}{2}, \frac{1}{2}, u)$. [At small $R$, where $(\Lambda, S)$ coupling dominates, the same curves would be designated $^2\Sigma_{g,1/2}$ and $^2\Pi_{u,1/2}$, $^2\Pi_{u,3/2}$ and $^2\Pi_{g,3/2}$, $^2\Pi_{g,1/2}$ and $^2\Sigma_{u,1/2}$, respectively.] The corresponding curves for $Ar_2^+$ have been computed by Johnson in an earlier work.[6]

As discussed by Johnson for $Ar_2^+$, the adiabatic states change from $(\Lambda, S)$ coupling at small $R$ to $(J_a, J_b)$ coupling at large $R$, there being an intermediate region where the exchange and spin-orbit energies are of about equal magnitude. The collision dynamics couples these fine-structure states

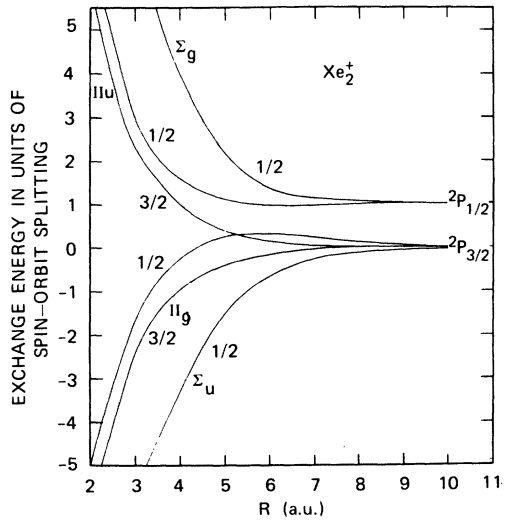


FIG. 1. Exchange energies for $Xe_2^+$ given in units of spin-orbit splitting (1.31 eV) as a function of internuclear separation $R$ in a.u. This figure is from the work of Johnson (Ref. 6).

and may produce transitions among them, particularly in the intermediate region. However, the location of the "nonadiabatic region" will depend upon the strength of the spin-orbit coupling and the velocity of the collision. At sufficiently high velocities or weak spin-orbit coupling, transitions will occur at long range and the spin-orbit coupling can be neglected. Conversely, at sufficiently low velocities and strong spin-orbit coupling, the collision will proceed adiabatically along the spin-orbit states, even into short range. In this work we examine these different limiting cases. In our energy range of 20–340 eV the $Xe^+$-on-Xe case appears to be entirely adiabatic even into the region where $(\Lambda, S)$ coupling dominates, whereas in the $Ar^+$-on-Ar case we observe mainly nonadiabatic collisions where spin and orbital angular momenta are decoupled, with indication of transition to an adiabatic regime at the lowest energies.

The present work presents measurements of the relative differential cross section for the direct elastic scattering of $Ar^+$ on Ar and $Xe^+$ on Xe in the energy range 20–340 eV and angular range 1–15 deg (lab). The argon data are an extension of earlier measurements made in this laboratory.[7] Our analysis of the argon data shows the observed interference pattern to be in excellent agreement with both a semiclassical and partial-wave calculation based upon the $\Pi_u$ and $\Pi_g$ energies of $Ar_2^+$ computed by Gilbert and Wahl[8] and Sidis.[9]

Our analysis of the xenon data has produced measured values of the *gerade-ungerade* pair-potential-energy difference, $\Delta V(R) \equiv |V_g(R) - V_u(R)|$, for two of the three pairs of coherent molecular fine-structure states of $Xe_2^+$. We consider these values to be in satisfactory agreement with those computed by Johnson,[5] while also being more accurate.

## II. APPARATUS AND EXPERIMENTAL PROCEDURE

The apparatus used for these measurements has been described in detail in an earlier work,[10] and the dimensions of the collimating apertures and their separation are unchanged. The electron bombardment energy in the ion source is 100 eV, so that the production of metastable ion states is energetically possible. Limits on the ratio of $Xe^+$ in the $^2P_{1/2}$ state to that in the $^2P_{3/2}$ (ground) state can be estimated as follows: Amme and Haugsjaa[11] measured this ratio to be 0.25 at an electron energy of 25 eV, the ratio increasing slowly with increasing energy. (If the two states were produced in statistical equilibrium, the ratio would be 0.50.) At our higher electron energy, we estimate the $^2P_{1/2}:{}^2P_{3/2}$ ratio to be about 0.40 for $Xe^+$, and nearly the same for $Ar^+$. Higher-lying metastable states are estimated to compromise less than 1% of the ion beam.

The scattered ions are energy analyzed electrostatically to select only the elastically scattered ions. The scattered ion current is amplified by an electron multiplier and an electrometer. The angular data are obtained by slow continuous scans at a rate consistent with good signal-to-noise ratio. The data are recorded on magnetic tape and are then processed by computer to yield plots of the reduced cross sections $\rho(\theta) \equiv \theta \sin\theta \sigma(\theta)$ versus the reduced angle $\tau \equiv E\theta$.[12] An absolute measurement of $\rho(\theta)$ was not attempted, due to the difficulty of determining detection sensitivity over wide ranges of scattered-particle flux and energy.

## III. DATA AND ANALYSIS

The theoretical basis for analyzing symmetric ion-atom scattering has been developed in a paper by Marchi and Smith,[13] and the results will be applied here. To review briefly, performing the Born-Oppenheimer separation of electronic and nuclear motions and treating the nuclear motion quantally, one obtains an amplitude for direct elastic scattering given by

$$f(\theta) = \tfrac{1}{2}[f_g(\theta) + f_u(\theta)], \tag{1}$$

where $f_g(\theta)$ and $f_u(\theta)$ are the (complex) scattered amplitudes from *gerade* and *ungerade* electronic molecular states, respectively. Each of these amplitudes can be represented as

$$f_{g,u}(\theta) = \sigma_{g,u}^{1/2}(\theta) e^{i\Phi_{g,u}}, \tag{2}$$

where the differential cross section $\sigma(\theta)$ can be computed classically for a particle moving in the appropriate potential field, and the phase $\phi_{g,u}$ can be computed as a classical action integral. Combining Eqs. (1) and (2) leads to

$$\sigma(\theta) = |f(\theta)|^2 = \tfrac{1}{4}\{\sigma_g(\theta) + \sigma_u(\theta) + 2\sigma_g^{1/2}(\theta)\sigma_u^{1/2}(\theta) \times \cos[\phi_g(\theta) - \phi_u(\theta)]\} , \quad (3)$$

or, equivalently,

$$\rho(\tau) = \tfrac{1}{4}\{\rho_g(\tau) + \rho_u(\tau) + 2\rho_g^{1/2}(\tau)\rho_u^{1/2}(\tau) \times \cos[\phi_g(\tau) - \phi_u(\tau)]\} . \quad (3a)$$

Since $\rho_g(\tau)$ and $\rho_u(\tau)$ are usually slowly varying functions of $\tau$, we expect the maximum in $\rho(\tau)$ to occur when

$$|\phi_g - \phi_u| = 2\pi N, \quad N = 1, 2, \ldots . \quad (4)$$

The quantal phases $\phi_g$ and $\phi_u$ are developed during the collision interaction and are given by an action integral over the classical motion, of the form

$$\phi_{g,u} = \int \epsilon_{g,u}\, dt . \quad (5)$$

The integration over time can be replaced by one over the path, $dt \to ds/v$. For small-angle scattering, the velocity $v$ can be treated as constant and proportional to $E^{1/2}$, and the integral over path will be nearly a function of $R_0$ or the impact parameter $b$ only, and hence of $\tau$ only. Thus Eq. (5) becomes, apart from constants,

$$\phi_{g,u} \sim E^{-1/2} \int \epsilon_{g,u}\, ds = E^{-1/2} F_{g,u}(\tau). \quad (6)$$

Combining Eqs. (4) and (6) gives, except for constants,

$$NE^{1/2} \sim |F_g(\tau) - F_u(\tau)| . \quad (7)$$

Therefore it is found that $NE^{1/2}$ is a direct measure of the difference potential $\Delta V(R)$.

The integer $N$ can be thought of as representing the number of round-trip excursions from target atom to incident ion and back to the target atom made by the unpaired electron during the collision. The fact that at constant $\tau$ the quantity $NE^{1/2}$ should remain constant provides a useful test for whether or not a pattern of oscillations in $\rho$-vs-$\tau$ plots can be attributed to phase interference between two coherent states. Equation (7) is also a convenient meeting ground between theory and experiment; experimentally determined values of $NE^{1/2}$ versus $\tau$ can be compared with computed values of the classical action integrals, derived from known or trial potential curves for the two states.

### A. $Ar^+$ on Ar

Figure 2 shows exemplary argon data at several selected energies. One or more runs were made at 5-eV intervals from 20 to 100 eV and at 20-eV intervals from 100 to 240 eV.

The most prominent features in these $\rho$-vs-$\tau$ plots are (i) the rainbow peak at $\tau \approx 115$ eV deg, independent of energy, and (ii) the interference peaks, which move with energy. The low-energy rainbow scattering is the subject of another paper.[14] In this paper we consider the interference patterns due to electron exchange symmetry.

At energies less than 100 eV there is, in ad-

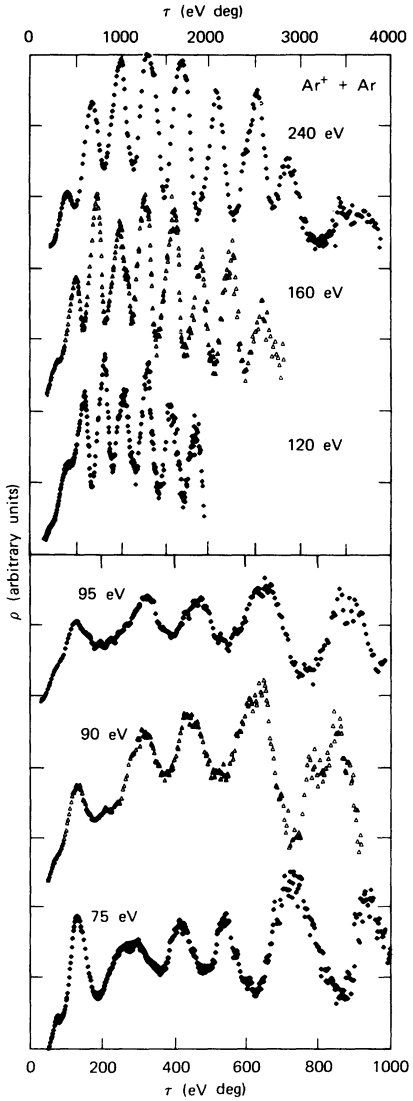


FIG. 2. Reduced plots of the experimental direct elastic scattering of $Ar^+ + Ar$ at selected laboratory collision energies.

dition to the regular pattern, a pronounced amplitude modulation of the oscillation, and also occasional broadening, narrowing, and asymmetry of peaks, suggesting the presence of a secondary "faster" oscillation which is unresolved in these measurements. Above 100 eV the oscillation is more regular, with larger amplitude and slight modulation.

The periodic property of the interference pattern over the entire experimental range is displayed in Fig. 3 and shows good agreement at 240 eV with earlier measurements on an entirely different apparatus.[1] (In the region of comparison, a minimum in the electron-capture probability $P_0$ corresponds to a maximum in $\rho$.) A best-fit empirical line is drawn through the data, each line representing a family of collisions for which the relative phase $|\phi_g - \phi_u|$ is a fixed integer $N$ times $2\pi$, as in Eq. (4). To determine the proper assignment of $N$ we use that set of $N$ values which at small angles ($3° < \theta < 8°$) make $NE^{1/2}$ constant (to within 1%) at constant $\tau$.

Figure 4 shows the experimental small-angle values of $NE^{1/2}$ versus $\tau$ obtained from Fig. 3. Also shown is the computed value, derived from the $^2\Pi_u$ and $^2\Pi_g$ interaction potentials of $Ar_2^+$ as calculated by both Gilbert and Wahl[8] ($4.2 \leq R \leq 5a_0$) and Sidis[9] ($1 \leq R \leq 4.5a_0$). (The two calculations are in excellent agreement in the overlap region; hence only one curve is shown in Fig. 4.) For the internuclear separation $2 \leq R \leq 5a_0$, the *ab initio* $\Pi$ potentials could be accurately represented by the exponential forms

$$V[^2\Pi_u](R) = 112.25e^{-1.6389R},$$
$$V[^2\Pi_g](R) = V[^2\Pi_u](R) - 7.5e^{-1.157R}. \quad (8)$$

Using these potentials, two scattering computations were done: a semiclassical action-integral type and a partial-wave type. Both of these fall on the curve shown. The agreement between experiment and theory is thus seen to be excellent—within 1 or 2%.

The above analysis indicates strongly that the major interference observed in these data is that due to the $\Pi$ states. We also observe an effect, particularly prominent in the 90-eV data, wherein the amplitude approximately doubles with increasing $\tau$. We believe this is caused by the mixing of fine-structure states at large $R$ with increasing energy, together with the increasing degeneracy of the $\Pi_{3/2}$ and the $\Pi_{1/2}$ states as the scattering probes smaller $R$ (larger $\tau$). As these two pairs of states become degenerate the phase differences and interference patterns become identical, causing the observed doubling in amplitude. The region of lower $\tau$, where the peak amplitude is low and the shapes irregular, is a complex region where the $\Pi$ states are not degenerate and where the transition between the two coupling regimes is occurring.

The faster oscillation, which apparently is present but mostly unresolved, is probably due to phase interference between the $\Sigma$ states of the orbital set. Theoretical calculations using the potentials of Gilbert and Wahl[8] and Sidis[9] indicate that the $\Sigma$-state oscillations should have a fre-

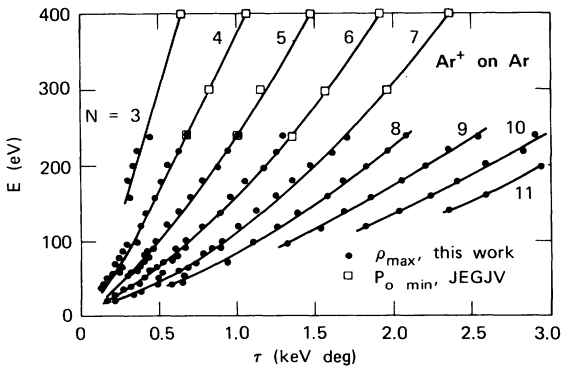


FIG. 3. Phase indexing of the $Ar_2^+$ elastic scattering maxima as a function of laboratory energy and $\tau$, including data from Ref. 1.

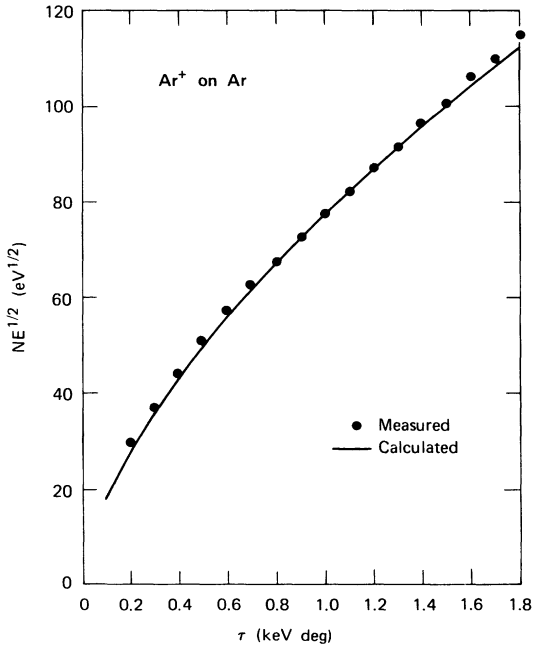


FIG. 4. $NE^{1/2}$-vs-$\tau$ plot for $Ar_2^+$. The solid circles are obtained from the analysis of the experimental cross sections and the line is from calculations using the $^2\Pi_g$ and $^2\Pi_u$ potential curves of Gilbert and Wahl (Ref. 8) and Sidis (Ref. 9).

quency approximately three to four times faster than the Π-state oscillations. The spacing of the Σ-state oscillations would therefore be at the angular and energy-resolution limits of the scattering apparatus. Moreover, this oscillation could be rather complex in the intermediate regime where some transitions among the fine-structure states are occurring.

### B. $Xe^+$ on Xe

Figures 5 and 6 show exemplary xenon data at selected energies. Runs were made at 5-eV intervals from 20 to 100 eV, 10-eV intervals from 100 to 200 eV, and 20-eV intervals from 200 to 340 eV. Additional runs were made at intermediate energies in several cases where the oscillatory pattern was changing rapidly with energy.

At low energies ($E \lesssim 50$ eV) the most prominent feature of the $\rho$-vs-$\tau$ plots is a large rainbow peak at $\tau \approx 93$ eV deg, and a smaller one at $\tau \approx 20$ eV deg, independent of $E$. These peaks are shown clearly in the data presented in Fig. 2 of Ref. 14. The rainbow peak at $\tau \approx 93$ eV deg is due to the potential well of the $(\frac{3}{2}, \frac{1}{2}, u)$ state with a depth of 0.97 eV. The rainbow peak at small angles, $\tau \approx 20$ eV deg, is probably due to a shallow well of approximately 0.25 eV on the $(\frac{1}{2}, \frac{1}{2}, u)$ state. Interference peaks can be seen at all energies, even in the rainbow region ($\tau \lesssim 93$ eV deg), moving with $E$. The complex interference pattern can be resolved into a primary (slow) oscillation and a secondary (fast) oscillation, the latter being unobservable at small angles due to inadequate angular resolution.

We believe the apparent rapid rise in $\rho$ at small $\tau$ is a small-angle instrumental effect; it corresponds to $\theta \lesssim 3$ deg (lab) and is associated with the particular geometry and finite angular spread of both the incident and scattered beams. Duplicate runs with different main-beam focusing have shown rather different slopes in this region, but yield good agreement for $\theta \gtrsim 3$ deg (lab). Data from this region, if used at all, must be treated with considerable discretion.

Figure 7 shows the $E$, $\tau$ dependence of the fast-oscillation component over the entire range of measurement. As in argon, each best-fit empirical line through the data represents a family of collisions for which the relative phase $|\phi_g - \phi_u|$ is a fixed integer $N$ times $2\pi$, and $N$ is chosen to make $NE^{1/2}$ constant at constant $\tau$ [see Eq. (7)]. (Of course, there is but one free choice of $N$ for the entire set of data, since $N$ must increase by unity from one line to the adjacent line at larger $\tau$, or smaller $E$.)

The slow-oscillation component was found to be strong at low $E$ and small $\tau$ (i.e., large $R_0$), where the fast component was no longer in evidence, and

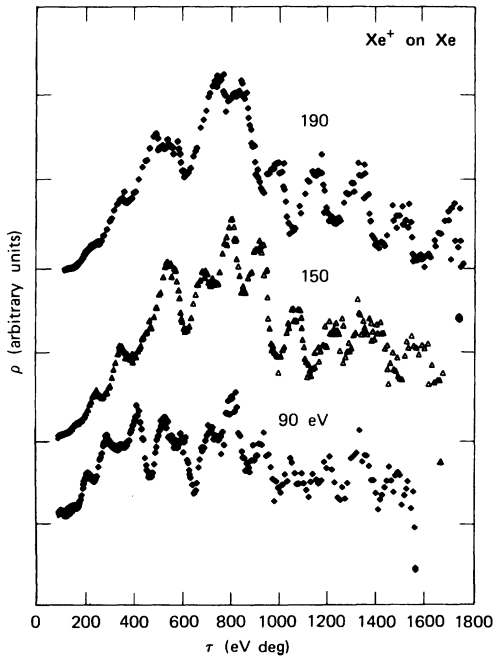


FIG. 5. Reduced plots of the experimental direct elastic scattering of $Xe^+ + Xe$ at several laboratory collision energies.

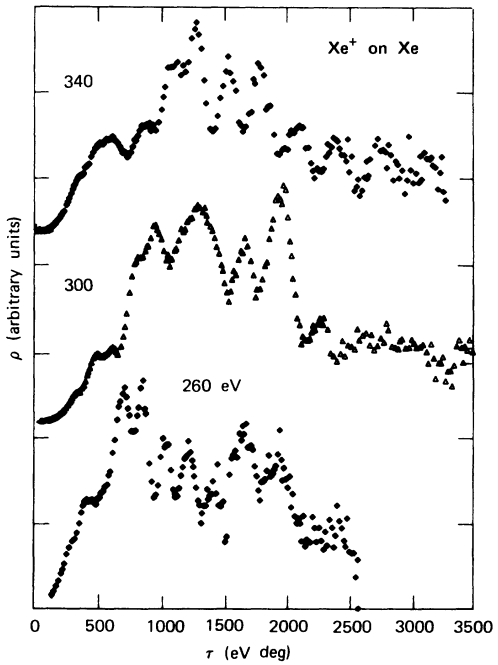


FIG. 6. Reduced plots of the experimental direct elastic scattering of $Xe^+ + Xe$ at several laboratory collision energies.

Fig. 8 shows its constant-phase plot over a rather large range of those two variables. In contrast to the corresponding plot for the fast component (Fig. 7), this plot shows significant irregularities—particularly for $\tau \gtrsim 1.2$ keV deg. In fact, we believe that some peaks plotted here are not pure interference peaks, but enhancement of scattering due to perturbation of a potential curve in the vicinity of a curve crossing.[15] Such an effect should be seen at nearly constant $\tau$ (constant $R_0$) independent of energy, and indeed many large peaks can be seen in the data at $\tau \approx 1.25$ keV deg. Furthermore, we estimate that this value of $\tau$ corresponds to a distance of closest approach, where the more repulsive scattering potentials are expected to cross the lowest excited-state curves.

The empirical lines of constant phase are not drawn for $\tau > 1.2$ keV deg, since in this region the complications of curve crossings make uncertain the identification of interference peaks. In fact, there is some indication that inelastic channels in this region greatly reduce the flux of elastically scattered particles in the states responsible for the slow-oscillation component.

In the region $0.8 < \tau < 1.2$ keV deg there is a small but significant shift in some of the lines of constant phase from the position required by a two-state interference pattern. There is also an amplitude modulation of the slow-oscillation peaks. The observed variations in phase and amplitude are consistent with a two-component slow oscillation, wherein the slow-oscillation component is itself the sum of two component oscillations of nearly the same (within ~30%) frequency and amplitude. This interpretation is consistent with the potential differences of Johnson[5] and indicates that the two similar oscillation components are from the $(\frac{1}{2}, \frac{1}{2})$ and $(\frac{3}{2}, \frac{1}{2})$ states.

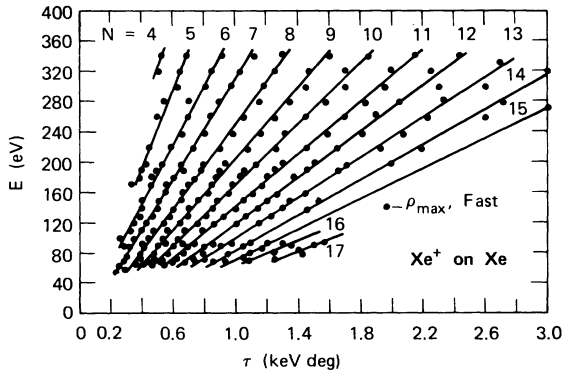


FIG. 7. Phase indexing of the fast $Xe_2^+$ elastic scattering maxima $(\frac{3}{2}, \frac{3}{2})$ as a function of laboratory energy and $\tau$.

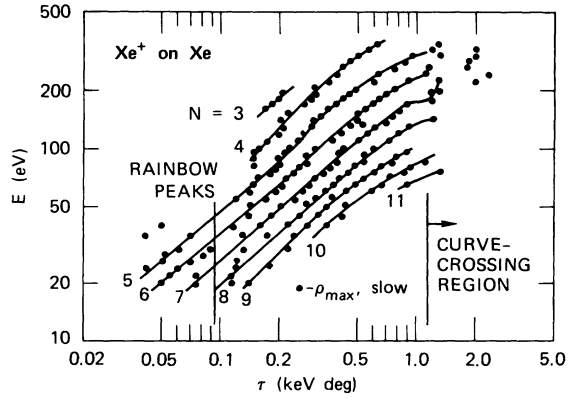


FIG. 8. Phase indexing of the slow $Xe_2^+$ elastic scattering maxima $(\frac{1}{2}, \frac{1}{2})$ as a function of laboratory energy and $\tau$.

Figure 9 shows the measured small-angle, values of $NE^{1/2}$ versus $\tau$, obtained from Figs. 7 and 8, for both the slow and fast oscillations. The slow-oscillation analysis is confined to the region $\tau < 0.8$ keV deg, where the constant-phase lines evidently can be attributed to a single pair of coherent states.

A difference potential $\Delta V(R) \equiv |V_g(R) - V_u(R)|$ was determined for the fast-oscillation data by using trial functions as part of *gerade* and *ungerade* scattering potentials:

$$V_{g,u}(R) = Ae^{-\alpha R} \pm \tfrac{1}{2}\Delta V_T(R) . \qquad (9)$$

The first term in the potential is the well-known exponential repulsion, recently discussed by Smith.[16] For $Xe^+$ we used[17] $A = 906$ and $\alpha = 1.889$,

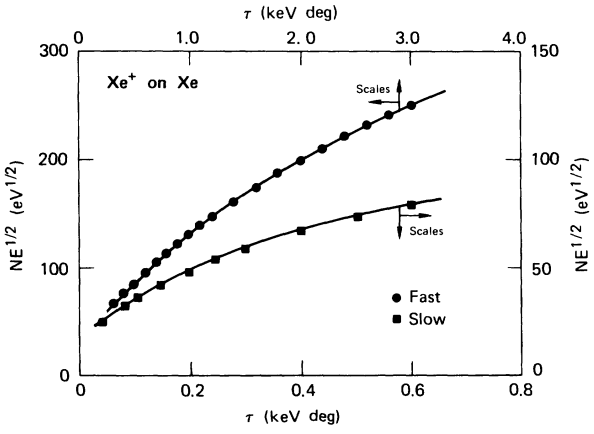


FIG. 9. $NE^{1/2}$-vs-$\tau$ plot for $Xe_2^+$. The solid circles are from the analysis of the fast oscillatory structure $(\frac{3}{2}, \frac{3}{2}$ states) and the solid squares are from the analysis of the slow oscillatory structure $(\frac{1}{2}, \frac{1}{2}$ states). The lines are calculated values using the potentials given by Eqs. (9)–(11).

in a.u. The trial functions $\Delta V_T(R)$ were also exponential. The function $NE^{1/2}(\tau)$ was obtained by computing the quantal phases $\phi_g$ and $\phi_u$ as action integrals over the classical trajectories corresponding to the interaction potentials $V_g(R)$ and $V_u(R)$, respectively.

The trial function $\Delta V_T(R)$ was varied to achieve satisfactory agreement between the computed function $NE^{1/2}(\tau)$ and the measured value shown in Fig. 9; the agreement achieved is everywhere better than 5%. Identifying the fast oscillation as being due to interference between the $(\frac{3}{2}, \frac{3}{2}, g)$ and $(\frac{3}{2}, \frac{3}{2}, u)$ states (which are also pure $\Pi_g$ and $\Pi_u$ states, respectively) yields the measured difference potential

$$\Delta V_{3/2,3/2}(R) = 23e^{-1.23R} \pm 10\%, \quad 3.5 \lesssim R \lesssim 5.5 \tag{10}$$

in a.u. (This assumes that the average potential is accurate to about 10%.)

A similar procedure was used to give a difference potential for the slow-oscillation component, which we identify with the $(\frac{1}{2}, \frac{1}{2}, g)$ and $(\frac{1}{2}, \frac{1}{2}, u)$ states. An additional exponential repulsive term was added to the scattering potential for the $(\frac{1}{2}, \frac{1}{2})$ states which had the functional form $6.1e^{-1.0733R}$. Such a term was obtained from the calculations of Johnson[5] and reflects the fact that the mean potential for these states is more repulsive than that for the $(\frac{3}{2}, \frac{3}{2}, g)$ and $(\frac{3}{2}, \frac{3}{2}, u)$ states, as shown in Fig. 1. The resulting difference potential, in a.u., is

$$\Delta V_{1/2,1/2}(R) = 2.0e^{-0.788R} \pm 10\%, \quad 5 \lesssim R \lesssim 6.5 . \tag{11}$$

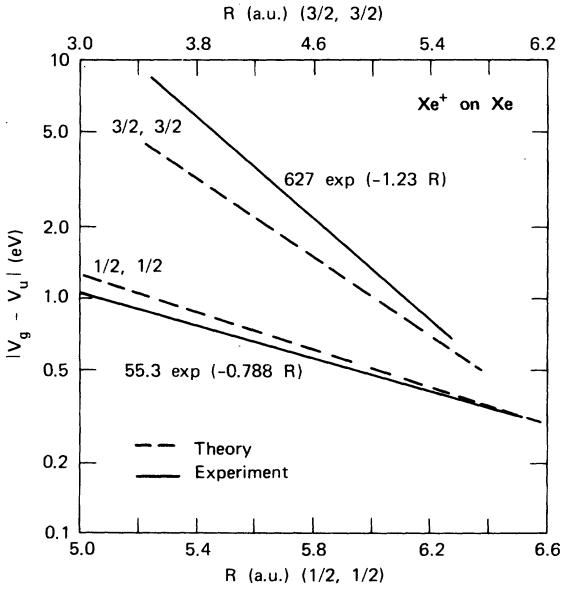


FIG. 10. Difference potentials for the $(\frac{3}{2}, \frac{3}{2})$ and $(\frac{1}{2}, \frac{1}{2})$ states of $Xe_2^+$ as a function of $R$. Solid curves are derived from the data. Broken curves are those calculated by Johnson (Ref. 5).

The comparison between these measured difference potentials and the calculations of Johnson (Fig. 1) is shown in Fig. 10. Since Johnson estimates his maximum error[18] at ±20% for $R \gtrsim 4$ a.u., and larger for $R < 4$ a.u., we consider the agreement to be quite satisfactory. In addition, Johnson recently has calculated a second-order $R^{-6}$ attractive contribution to the $Xe_2^+$ interaction[18] and finds it lowers his calculated $\Delta V_{1/2,1/2}(R)$ function by about 5% at $R = 5$ a.u., giving even better agreement with the measured value.

The identification of the fast- and slow-oscillation components of the data with the difference potentials $\Delta V_{3/2,3/2}(R)$ and $\Delta V_{1/2,1/2}(R)$, respectively, is based upon the following considerations: The amplitude of interference oscillations is proportional to $\rho_g^{1/2}(\theta)\rho_u^{1/2}(\theta)$, as shown in Eq. (3a), so that one expects the largest amplitude, observed in the slow oscillation, to come from the highly repulsive $(\frac{1}{2}, \frac{1}{2})$ curves (upper pair of curves in Fig. 1), provided the $^2P_{1/2}$ component of the ion beam is not too much less than the statistical equilibrium fraction. Similarly, the attractive $(\frac{3}{2}, \frac{1}{2}, u)$ curve ($\Sigma_u$ at small $R$) has a relatively small scattering cross section at small $\tau$ (except in the rainbow region), which would account for the apparent absence of a third oscillation component due to the $(\frac{3}{2}, \frac{1}{2})$ states. Also, the extension of the slow-oscillation pattern through the rainbow region is a further indication that neither of the two interfering states is the attractive $(\frac{3}{2}, \frac{1}{2}, u)$ state responsible for the rainbow scattering at $\tau \approx 93$ eV deg; the interference pattern from a coherent pair of potential curves, one of which has a well and produces rainbow scattering, becomes very complex and mostly unobservable at usual experimental resolution.

The aberrations of the slow-oscillation pattern in the region $0.8 < \tau < 1.2$ keV deg, noted previously, are attributed to the "missing" oscillation component from the $(\frac{3}{2}, \frac{1}{2})$ states. Calculations based upon Johnson's exchange energies (Fig. 1) and the repulsive potential of Eq. (9) show the factor $\rho_g^{1/2}(\theta)\rho_u^{1/2}(\theta)$ [Eq. (3a)] increasing with increasing $\tau$ relative to that for the $(\frac{1}{2}, \frac{1}{2})$ states, and predict comparable amplitudes of oscillation from both pairs of states in this region. Furthermore, the calculated period $\Delta\tau$ of the $(\frac{3}{2}, \frac{1}{2})$ oscil-

lation is only about 25% smaller than that of the $(\frac{1}{2}, \frac{1}{2})$ oscillation in this region, so that the effect of the additional oscillation would be to shift the peaks (and valleys), and modulate the amplitude of the other oscillation. Unfortunately, the data in this region are insufficient to derive the two pair potentials $\Delta V_{1/2,1/2}(R)$ and $\Delta V_{3/2,1/2}(R)$.

ACKNOWLEDGMENTS

We are indebted to Dr. R. E. Johnson for several valuable discussions, and for making numerical values of his computations available to us. We also are grateful to Dr. F. T. Smith for supplying the xenon repulsive potential, and for general encouragement of this work.

---

*Work supported by the U. S. Army Research Office (Durham, N. C.).

†On leave from the University of Massachusetts, Amherst, Mass.

[1]P. R. Jones, N. W. Eddy, H. P. Gilman, A. K. Jhaveri, and G. Van Dyk, Phys. Rev. 147, 76 (1966).

[2]William Aberth and D. C. Lorents, Phys. Rev. 144, 109 (1966).

[3]M. Barat, J. Baudon, M. Abignoli, and J. C. Houver, J. Phys. B 3, 230 (1970).

[4]P. R. Jones, T. L. Batra, and H. A. Ranga, Phys. Rev. Lett. 17, 281 (1966).

[5]R. E. Johnson, J. Phys. Soc. Japan 32, 1612 (1972).

[6]R. E. Johnson, J. Phys. B 3, 539 (1970).

[7]W. Aberth and D. C. Lorents, Phys. Rev. 144, 109 (1966).

[8]T. L. Gilbert and A. C. Wahl, J. Chem. Phys. 55, 5247 (1971).

[9]V. Sidis, in *Proceedings of the Eighth International Conference on the Physics of Electron-Atom Collisions*, edited by B. C. Čobić and M. V. Kurepa (Institute of Physics, Beograd, Yugoslavia, 1973), p. 200.

[10]D. C. Lorents and W. Aberth, Phys. Rev. 139, A1017 (1965).

[11]R. C. Amme and P. O. Haugsjaa, Phys. Rev. 165, 63 (1968).

[12]F. T. Smith, R. P. Marchi, and K. G. Dedrick, Phys. Rev. 150, 79 (1966).

[13]R. P. Marchi and F. T. Smith, Phys. Rev. 139, A1025 (1965).

[14]D. C. Lorents, R. E. Olson, and G. M. Conklin, Chem. Phys. Lett. 20, 589 (1973).

[15]See F. T. Smith, D. C. Lorents, W. Aberth, and R. P. Marchi [Phys. Rev. Lett. 15, 742 (1965)] for a description of this effect.

[16]Felix T. Smith, Phys. Rev. A 5, 1708 (1972).

[17]Suggested by Felix T. Smith (private communication).

[18]R. E. Johnson (private communication).